

Transcritical two-layer flow over topography

By W. K. MELVILLE AND KARL R. HELFRICH†

Massachusetts Institute of Technology, Cambridge, MA 02139, USA

(Received 4 February 1986 and in revised form 25 August 1986)

The evolution of weakly-nonlinear two-layer flow over topography is considered. The governing equations are formulated to consider the effects of quadratic and cubic nonlinearity in the transcritical regime of the internal mode. In the absence of cubic nonlinearity an inhomogeneous Korteweg–de Vries equation describes the interfacial displacement. Numerical solutions of this equation exhibit undular bores or sequences of Boussinesq solitary waves upstream in a transcritical regime. For sufficiently large supercritical Froude numbers, a locally steady flow is attained over the topography. In that regime in which both quadratic and cubic nonlinearity are comparable, the evolution of the interface is described by an inhomogeneous extended Korteweg–de Vries (EKdV) equation. This equation displays undular bores upstream in a subcritical regime, but monotonic bores in a transcritical regime. The monotonic bores are solitary wave solutions of the corresponding homogeneous EKdV equation. Again, locally steady flow is attained for sufficiently large supercritical Froude numbers. The predictions of the numerical solutions are compared with laboratory experiments which show good agreement with the solutions of the forced EKdV equation for some range of parameters. It is shown that a recent result of Miles (1986), which predicts an unsteady transcritical regime for single-layer flows, may readily be extended to two-layer flows (described by the forced KdV equation) and is in agreement with the results presented here.

Numerical experiments exploiting the symmetry of the homogeneous EKdV equation show that solitary waves of fixed amplitude but arbitrary length may be generated in systems described by the inhomogeneous EKdV equation.

1. Introduction

In a series of recent papers (Wu & Wu 1982; Akylas 1984; Mei 1986; Cole 1985) a number of authors have studied the transcritical forcing of nonlinear long waves by surface pressure or bottom topographic perturbations. In each case solitary waves of elevation have been found to evolve upstream of the forcing for some range of Froude numbers and forcing strength. Thus it appears, that for a certain parametric range, steady solutions may not be found for this class of problems (Miles 1986).

In this paper we examine the transcritical flow of a two-layer fluid over bottom topography. In many respects this particular problem is a very good example of this class of problems since we expect transcritical conditions to be relatively common in meteorology and oceanography. In addition, the generation of internal solitary waves by flow over topography has been a controversial subject in coastal oceanography (Lee & Beardsley 1974; Maxworthy 1979), a context in which this generation mechanism has not been considered. Further, unlike the problems cited above, there

† Present address: Woods Hole Oceanographic Institution, Woods Hole, MA 02543, USA.

are at least two types of lowest mode solitary waves for a stratified flow (Kakutani & Yamasaki 1978; Miles 1979). The first is a generalization of the Boussinesq solitary wave of the single-layer fluid, while the second is a monotonic non-dissipative bore between two regions of steady flow. This second type occurs at a parametric limit in that regime in which cubic nonlinearity is comparable to quadratic nonlinearity. In the absence of this second type of wave many of the results for transcritical forcing of a single-layer free-surface flow carry over to the two-layer fluid. It is the presence of the non-dissipative bore for this class of problems that is the primary novel feature of this study.

This work also bears on the problem of upstream influence in stratified flows that has been studied since the work of Long (1954). In this context the problem is to determine whether a steady flow over topography, which is calculated from known upstream conditions, is an asymptotic solution to an initial-value problem, or whether disturbances associated with the topography can propagate far upstream leading to new steady conditions just upstream of the topography. Baines (1984) has recently presented an extensive study of two-layer flow over topography based on hydraulic theory and laboratory experiments; using the experimental data to guide the class of solutions sought. Internal hydraulic jumps and drops are modelled by shock solutions; however, the nonlinear hydraulic theory does not account for the effects of dispersion that are evident in the experiments.

The results presented here complement the modelling of Baines (1984). The weakly nonlinear dispersive model cannot account for breaking and hydraulic jump/drop formation, whereas the nonlinear hydraulic model cannot account for the dispersive effects. Of particular interest to the present study is Baines' (1984) observation of a laminar, upstream bore that 'mainly consisted of a forward face which propagated without discernable change in shape'. Using results of the KdV theory of Benjamin (1966) Baines conjectured 'that steady-state inviscid bores are not possible in two-layer or stratified finite-depth systems, and that attempts to set up such a bore will result in the continuous production of a sequence of solitary waves. This conjecture is far from proven, however.' We will return to Baines' conjecture in §5.

Here we present a theoretical and experimental study of transcritical two-layer flow over topography in that regime in which the effects of weak nonlinearity, dispersion, topography and the near-critical Froude number all enter at the highest order. The resulting equation is either a forced KdV equation or extended KdV equation which includes cubic nonlinearity. The equations are derived in §2. Experimental and numerical techniques are described in §3 and the results presented in §4.

During final preparation of this paper we became aware of recent theoretical and numerical work by Grimshaw & Smyth (1986) and Smyth (1987) which anticipates some of the results of this work for the inhomogeneous KdV equation (§4.3) but does not consider the effects of cubic nonlinearity. A comparison of our results with theirs is given in §5.

2. Forced evolution equation

The two-layer flow has an equilibrium interface at $y^* = 0$, and upper and lower boundaries at $y^* = d_+^*$ and $y^* = d_-^* + H^*(x^*)\mathcal{H}(t^*)$, respectively, where $\mathcal{H}(t^*)$ is the Heaviside unit step function. In the absence of the bottom topography (i.e. $t^* < 0$) the basic flow is in the positive x -direction with a speed U in both layers.

The non-dimensional governing equations for two-layer inviscid incompressible, irrotational flow with an interface at $y^* = \eta^*(x^*, t^*)$ are

$$\beta\phi_{xx} + \phi_{yy} = 0 \quad (y \neq \alpha\eta), \quad (2.1)$$

$$\eta_t + F\eta_x + \alpha\phi_{\pm x}\eta_x = \frac{1}{\beta}\phi_{\pm y} \quad (y = \alpha\eta), \quad (2.2)$$

$$\rho_+ \left\{ \phi_{+t} + \frac{1}{\sigma}\eta + F\phi_{+x} + \frac{1}{2} \left(\alpha\phi_{+x}^2 + \frac{\alpha}{\beta}\phi_{+y}^2 \right) \right\} - \rho_- \left\{ \phi_{-t} + \frac{1}{\sigma}\eta + F\phi_{-x} + \frac{1}{2} \left(\alpha\phi_{-x}^2 + \frac{\alpha}{\beta}\phi_{-y}^2 \right) \right\} = 0 \quad (y = \alpha\eta), \quad (2.3)$$

$$\phi_{+y} = 0 \quad (y = d_+), \quad (2.4)$$

$$\phi_{-y} = \frac{\gamma\beta}{\alpha} [F + \alpha\phi_{-x}] H_x \quad (y = d_- + \gamma H), \quad (2.5)$$

where the dimensional variables, denoted by an asterisk are related to the dimensionless variables by

$$\left. \begin{aligned} x^* &= lx, & y^* &= h_0 y, & t^* &= \frac{lt}{c_0}, \\ \eta^* &= a\eta, & \phi^* &= \frac{\sigma g l a}{c_0} \phi, & \rho^* &= \rho_0 \rho, & d_{\pm}^* &= \frac{d_{\pm}^*}{h_0}, \\ \sigma &= \frac{\rho_-^* - \rho_+^*}{\rho_0}, & c_0^2 &= \sigma g h_0, & H^* &= H_0 H, \\ \alpha &= \frac{a}{h_0}, & \beta &= \left(\frac{h_0}{l} \right)^2, & \gamma &= \frac{H_0}{h_0}, \\ F &= \frac{U}{c_0} = 1 + \epsilon, & h_0 &= \frac{d_+^* d_-^*}{(d_+^* + d_-^*)}. \end{aligned} \right\} \quad (2.6)$$

The characteristic height and length of the topography are H_0 and l , respectively. The characteristic depth of the fluid is h_0 , ρ_0 is a characteristic density, and c_0 is the phase speed of linear non-dispersive long waves. The characteristic displacement of the interface is a . The parameters α , β , γ and ϵ are small by hypothesis. The parameter β , which measures dispersion, scales according to

$$\beta = O(\alpha), \quad D \equiv \frac{|d_- - d_+|}{d_+ + d_-} = O(1), \quad (2.7)$$

$$= O(\alpha^2), \quad D = O(\alpha), \quad (2.8)$$

where α is a measure of nonlinearity (cf. Helfrich, Melville & Miles 1984). The parameter ϵ which measures the departure of the Froude number from unity is $O(\beta)$. The parameter γ which measures the height of the topography is given by

$$\gamma = \alpha\beta B, \quad (2.9)$$

where the parameter B is $O(1)$. This scaling ensures that each of nonlinearity, dispersion, topography and transcritical effects enters at the highest order.

The forced evolution equation is obtained by expanding the solutions for $\phi(x, y, t)$, which satisfy (2.1), (2.4) and (2.5) in powers of β to give

$$\phi_+ = \Phi_+(x, t) - \beta(\frac{1}{2}y^2 - d_+ y) \frac{\partial^2 \Phi_+}{\partial x^2} + \beta^2 (\frac{1}{24}y^4 - \frac{1}{8}d_+ y^3 + \frac{1}{3}d_+^3 y) \frac{\partial^4 \Phi_+}{\partial x^4} + O(\beta^3), \quad (2.10)$$

$$\begin{aligned} \phi_- = \Phi_-(x, t) - \beta(\frac{1}{2}y^2 + d_- y) \frac{\partial^2 \Phi_-}{\partial x^2} \\ + \beta^2 \left[(\frac{1}{24}y^4 + \frac{1}{8}d_- y^3 - \frac{1}{3}d_-^3 y) \frac{\partial^4 \Phi_-}{\partial x^4} + BFy \frac{dH}{dx} \right] + O(\beta^3, \gamma\beta), \end{aligned} \quad (2.11)$$

and then following Whitham's (1974, §13.11) derivation of the Korteweg-de Vries equation,† but retaining both quadratic and cubic nonlinear terms.

Since we are interested in the upstream conditions we restrict the solution to waves moving in the negative x -direction relative to the undisturbed flow. In addition, to ensure that the boundary condition (2.4) is a consistent approximation to a free surface, we assume that $\sigma \ll 1$. The final evolution equation then becomes,

$$\eta_t + (F-1)\eta_x - \frac{3}{2}\alpha(d_{-2}\eta - 2\alpha d_{-3}\eta^2)\eta_x - \frac{1}{6}\beta d_1 \eta_{xxx} = \frac{\beta BF}{2d_-} H_x + O(\alpha\beta), \quad (2.12)$$

where

$$d_n = \{d_-^n + (-)^{n-1}d_+^n\}. \quad (2.13)$$

As a result of Galilean invariance of the dynamics, the homogeneous form of (2.12) could have been anticipated. The right-hand side represents the topographic forcing, in which F may be set to unity; an approximation that is consistent with the neglected higher-order terms.

Equation (2.12) may be recast in terms of new (primed) variables

$$\eta' = \frac{\eta}{\lambda}, \quad \tau' = \frac{t}{\zeta}, \quad \chi' = \frac{x - (F-1)t}{\xi}, \quad (2.14)$$

to give (dropping the primes)

$$\eta_\tau - 24\eta(1-\eta)\eta_\chi - \eta_{\chi\chi\chi} = \nu H_\chi, \quad (2.15)$$

where

$$\left. \begin{aligned} \lambda &= \frac{d_{-2}}{2\alpha d_{-3}}, \\ \zeta &= \frac{128}{d_{-2}^3} (\frac{1}{3}\beta d_1 d_{-3}^3)^{\frac{1}{2}}, \\ \xi &= \frac{4}{d_{-2}} (\frac{1}{3}\beta d_1 d_{-3}^3)^{\frac{1}{2}}, \\ \nu &= \frac{32\alpha\beta d_{-3}^2 BF}{d_- d_{-2}^3}. \end{aligned} \right\} \quad (2.16)$$

and

† Following Whitham, the kinematic conditions and dynamic condition at the interface can be written in terms of η and the vertically-averaged horizontal velocities in both layers \bar{u}_\pm . The kinematic conditions can then be used to obtain a relationship $\bar{u}_- = \bar{u}_-(\bar{u}_+, \eta)$ which when substituted into the dynamic condition gives two equations in \bar{u}_+ and η . The subsequent steps then exactly parallel Whitham's procedure.

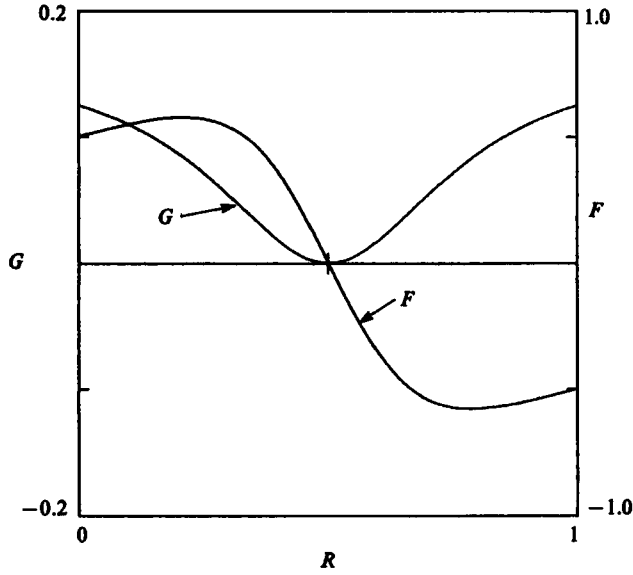


FIGURE 1. Amplitude and nonlinear speed corrections for monotonic bore solution, F and G , respectively, as functions of R , the ratio of the lower-layer depth to total depth.

Kakutani & Yamasaki (1978), and Miles (1979), have shown that the homogeneous form of (2.16) admits a family of solitary wave solutions given by

$$\eta(\chi, \tau; \mu) \equiv \eta_\mu = 2\mu(1 + \mu)^{-1} [\cosh^2 \theta - \mu \sinh^2 \theta]^{-1}, \quad (2.17a)$$

$$\theta = \kappa\chi + 4\kappa^2\tau + \theta_0, \quad \kappa = 2\mu^{\frac{1}{2}}(1 + \mu)^{-1}, \quad (2.17b, c)$$

and η is real and bounded for $-\infty < \theta < \infty$ for $0 < \mu < 1$ with θ_0 real.

They also found the isolated solution

$$\eta(\chi, \tau; 1) \equiv \eta_1 = \frac{1}{2}(1 + \tanh \theta), \quad (2.18a)$$

$$\theta = \chi + 4\tau + \theta_1, \quad (2.18b)$$

which corresponds to a non-dissipative bore. It is the presence of this second class of permanent-form solutions which motivated this study and distinguishes it from the other recent studies of transcritical forcing.

From (2.17) and (2.18) it may be seen that the maximum solitary wave speed occurs for $\mu = 1$ and (from (2.14), (2.16) and (2.18b)) is given by

$$c_{\max} = c_0(1 + G(R)), \quad (2.19a)$$

where
$$G(R) = \frac{(1 - 2R)^2}{8(1 - 3R + 3R^2)}; \quad (2.19b)$$

and
$$R = \frac{d_-}{(d_+ + d_-)},$$

is the ratio of the depth of the lower layer to the total depth.

It is well known that the homogeneous form of (2.16) admits solitary wave solutions

of elevation (depression) for $R < \frac{1}{2}$ ($> \frac{1}{2}$). For each $R < \frac{1}{2}$ ($> \frac{1}{2}$) there exists one and only one monotonic bore solution of elevation (depression) having an amplitude

$$a = h_0 F(R)^\dagger, \quad (2.20a)$$

where

$$F(R) = \frac{1}{2} \frac{(1-2R)}{(1-3R+3R^2)}. \quad (2.20b)$$

Curves of $G(R)$ and $F(R)$ are shown in figure 1.

3. Experimental methods

The experiments were carried out in the tilting glass flume at the R. M. Parsons Laboratory, MIT. The flume was set in a horizontal position and the ends sealed to provide a working section 15 m long by 0.45 m wide, with a nominal depth of 0.15 m. Following Baines (1984), the two-layer experiments were carried out with an upper layer of dyed kerosene ($\rho = 0.80 \text{ g/cm}^3$) and a lower layer of fresh water ($\rho = 0.986 \text{ g/cm}^3$).

The forcing was imposed by an inverted sech^2 -shaped \ddagger lucite topography mounted to a carriage and immersed in the upper (kerosene) layer. The carriage was driven by a stepper motor controlled by a variable frequency generator. In a typical experiment the carriage was positioned at one end of the channel, accelerated under manual control for approximately 5 seconds and thereafter run at constant speed until it reached the opposite end of the channel.

The flow was monitored at two stations. At the first station encountered by the carriage (5 m downstream of the starting location of the centre of the topography), the displacement of the interface was measured using a Reticon camera that gave an analogue output proportional to the displacement of the dark/light transition between the essentially opaque kerosene and translucent water. In some experiments it was not possible to image a single transition over the dynamic range of the Reticon camera and this led to ambiguity and 'drop-out' of the analogue signal. This drop-out was considered acceptable as the primary use of the data at this station was to give a reference time which, with the velocity data at the second station, permitted us to measure the speed of the disturbance. This data is included in figures 5 and 10 since it does provide more than just timing information.

The resolution of the camera was in the range 10^{-2} – 10^{-1} mm. At a second station 9.25 m from the starting position, a Disa laser anemometer was used to measure the horizontal velocity in the water, 5 cm from the bottom of the channel. At the same station still photographs were taken with a Hasselblad 500 ELM camera for comparison with the velocity measurements.

The analogue signals from both the Reticon camera and laser anemometer were digitally sampled at 20 Hz and stored for later processing. The analogue signals were also displayed on a digital oscilloscope from which preliminary measurements (e.g. travel times between stations) could be made to confirm the quality of the data.

\dagger Equation (2.20a) was also used to define the amplitude parameter, a , in (2.6), and the apparently large values of a in the examples considered below follow in part from this convention.

\ddagger $H = H_0 \text{sech}^2 Kx$, $H_0 = 5.1 \text{ cm}$, $K = 0.039 \text{ cm}^{-1}$.

4. Results

4.1. Numerical solutions: extended forced KdV equation ($R = 0.35$)

Numerical† solutions were obtained for a range of forcing strengths and Froude numbers with qualitatively different results. Figure 2 shows a sequence of interfacial displacements as functions of x and T ($T = \frac{1}{6}\beta d_1 t$) for $(F, R, \alpha, \beta, \gamma) = (0.95, 0.35, 0.472, 0.0154, 0.055)$. Here the solutions show an undular bore evolving upstream leading to a new upstream elevation, with a depression following the topography and a trailing wavetrain.

The qualitative form of the solution depends on the Froude number and the strength of the forcing as shown in figure 3. This figure displays solutions at the same $T (= 2.5)$, for α, β, γ and R fixed, and $F = 0.95, 1.0, 1.1$, respectively. With the increase in F , the solution goes from an undular bore upstream, to a monotonic bore, then to a steady supercritical solution. The first two of these solutions are globally unsteady but do ultimately give new locally steady conditions immediately upstream of the topography. The monotonic bore solution is clearly obtained, and, to within the accuracy of the numerical solutions, has the amplitude and speed of the corresponding homogeneous solution. Figure 4 summarizes the qualitative form of the transcritical solutions of the forced EKdV equation in the (F, γ) plane. The monotonic bore solution imposes the maximum speed at which disturbances can propagate upstream. This then provides a constant Froude number boundary between steady supercritical flow over the topography (cf. figure 3) and the monotonic bore solution. As F is reduced with γ fixed, the upstream disturbance changes to the undular bore. As a result of the finite run times it is not clear whether there is a sharp transition from monotonic to undular bore and we have marked a narrow transition region on the figure. A further decrease in F leads to a transition from an undular bore upstream to a solution with no permanent upstream influence in the neighbourhood of the topography.

4.2. Two-layer experimental and numerical results ($R = 0.33$)

Experiments were run with $R = 0.33$ and F in the range $[0.73, 1.14]$ and examples of the interfacial displacement and velocity in the lower layer are shown in figure 5. The gaps in the time series of the interfacial displacement are due to the drop-out discussed above. Figure 5(a) ($F = 0.73$) shows good agreement between measurements and predictions of the upstream disturbances. The two numerical curves correspond to setting $F = 0.73$ or 1 in the forcing term (cf. (2.12)), both of which are consistent with the order of the neglected terms in the approximate theory. The predictions of the disturbance downstream of the topography show only qualitative agreement. Figures 5(b) and 5(c) ($F = 0.83$ and 0.94 , respectively) show good agreement on the length of the upstream disturbance but only qualitative agreement on the shape. Again, the downstream disturbance shows qualitative agreement. Figure 5(d) ($F = 1.09$) shows good quantitative agreement, with the primary disturbance now essentially locked to the topography. The prediction of the amplitude of the plateau downstream of the topography has improved. The amplitudes of the trailing waves are poorly predicted but in view of our neglect of downstream travelling waves this is not surprising.

It is of interest to note, especially in figure 5(c), the gradual increase in depth of

† Solutions were computed using the explicit finite-difference scheme of Vleighhart (1971), with straightforward extensions to include the cubic term. In all numerical experiments the bottom topography is given by $H = 1 - 4x^2$ for $|x| < 0.5$.

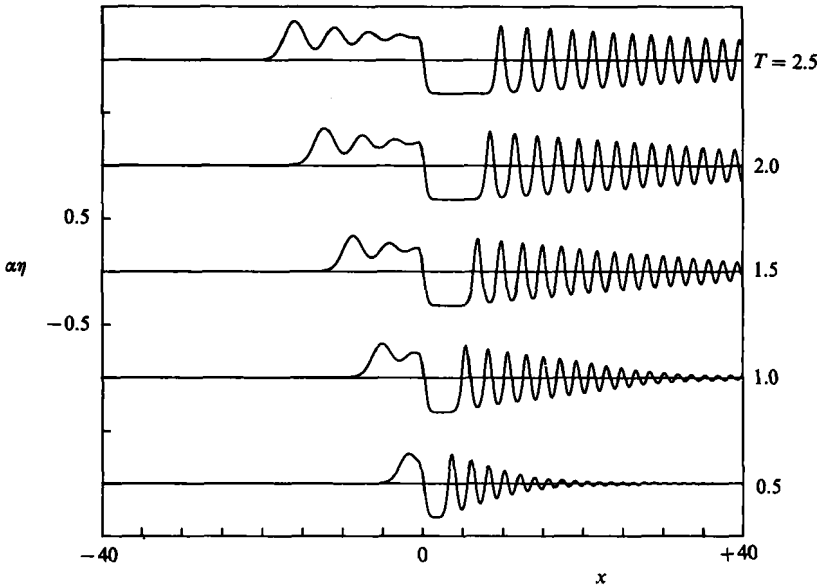


FIGURE 2. Example of undular bore evolving upstream in solution of (2.12) at various times T , with $(F, R, \alpha, \beta, \gamma) = (0.95, 0.35, 0.472, 0.0154, 0.055)$.

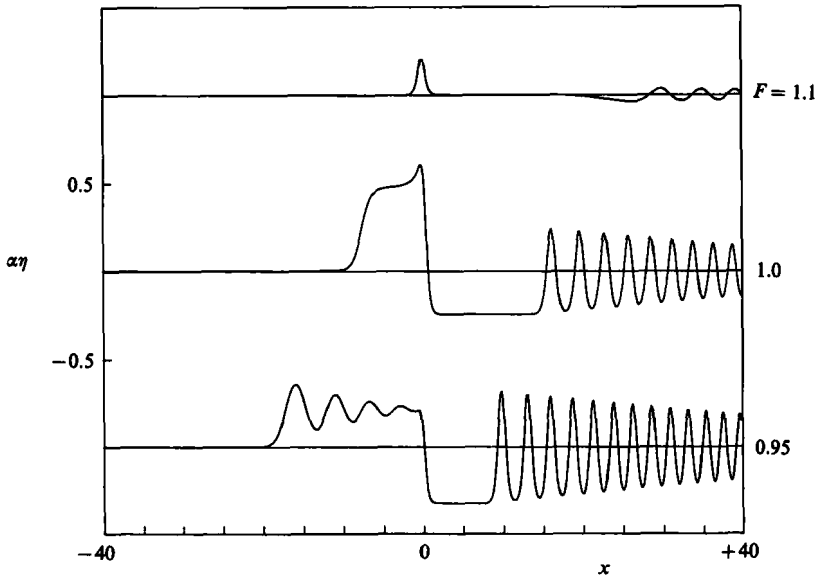


FIGURE 3. Examples of three classes of solution to (2.12) (steady supercritical, monotonic upstream bore, undular upstream bore) at $T = 2.5$ for various F with $(R, \alpha, \beta, \gamma) = (0.35, 0.472, 0.0154, 0.055)$.

the upper layer following the front of the upstream disturbance. Baines (1984) interpreted such features as 'rarefactions'.

Figure 6 shows the experimental measurements of the excess upstream† disturbance speed relative to the linear long wave speed for two topographic heights $\gamma = (0.3, 0.6)$. Also shown are the excess speed of the dissipationless bore and the locus of speeds for disturbances locked to the topography. The experiments show that the

† Upstream here also includes the limiting case of a disturbance locked to the topography.

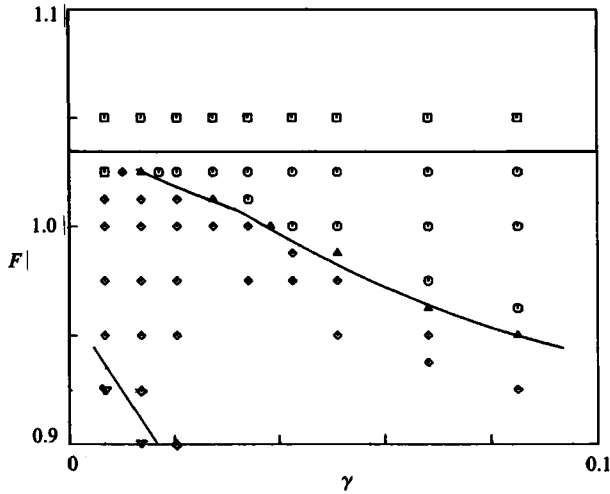


FIGURE 4. Regions in (F, γ) -plane occupied by \square , locally steady supercritical solution; \circ , monotonic upstream bore and \diamond , undular upstream bore; and ∇ , no local upstream influence. Symbol, \triangle , marks a transition solution between \circ and \diamond . $(R, \alpha, \beta) = (0.35, 0.472, 0.0154)$.

measured excess speeds are essentially independent of the topographic height for the two cases considered and increase from 0.038 ($F = 0.73$) to 0.085 ($F = 1.09$) compared to the constant predicted-weakly-nonlinear excess bore speed of 0.043. For larger F the primary disturbance is locked to the topography.

This quantitative disagreement with the theoretical results is most likely due to higher-order nonlinear effects resulting from the relatively large penetration of the topography. This is supported by figure 7 where we have plotted $\alpha\eta_{\max}$, the maximum dimensionless upstream interfacial displacement, as a function of F . Over the range of F considered, $\alpha\eta_{\max}$ is in the range (0.3, 1.0) whereas we have assumed $\alpha\eta \ll 1$ in the weakly nonlinear theory.

4.3. Numerical solutions: forced KdV equation ($R = 0.2$)

A number of numerical runs were made for the forced KdV equation (equation (2.12) with the cubic term neglected) with $R = 0.2$. Although the context here is different (internal waves), similar results are reported by Mei (1986) for the same generic model applied to ship hydrodynamics. In figure 8 we show examples of the three qualitatively different solutions obtained at $T = 0.5$ for different values of F with α, β, γ fixed. The undular bore and locally steady supercritical solutions are qualitatively the same as the corresponding results for the forced EKdV equation (cf. figure 3); however, the intermediate solution, the sequence of solitary waves of constant amplitude, replaces the monotonic bore solution of the forced EKdV equation.

The regions in which these solutions are found in the (F, γ) -plane are shown in figure 9 for $T \leq 2$ (cf. figure 4). The transition, from solitary waves upstream to supercritical flow, is from an unsteady to steady flow in the neighbourhood of the obstacle, and corresponds to the upper critical Froude number, F_u , of Miles (1986). It is shown in the Appendix that Miles' prediction of F_u for a single-layer flow is readily extended to two layers and given by (A 3). Thus we have plotted F_u in figure 9. The agreement between the predicted F_u and that obtained from the numerical solutions is within the uncertainty introduced by the neglected higher-order terms (cf. §4.2).

We have also plotted flow regime boundaries derived by Grimshaw & Smyth (1986), which are discussed in §5.

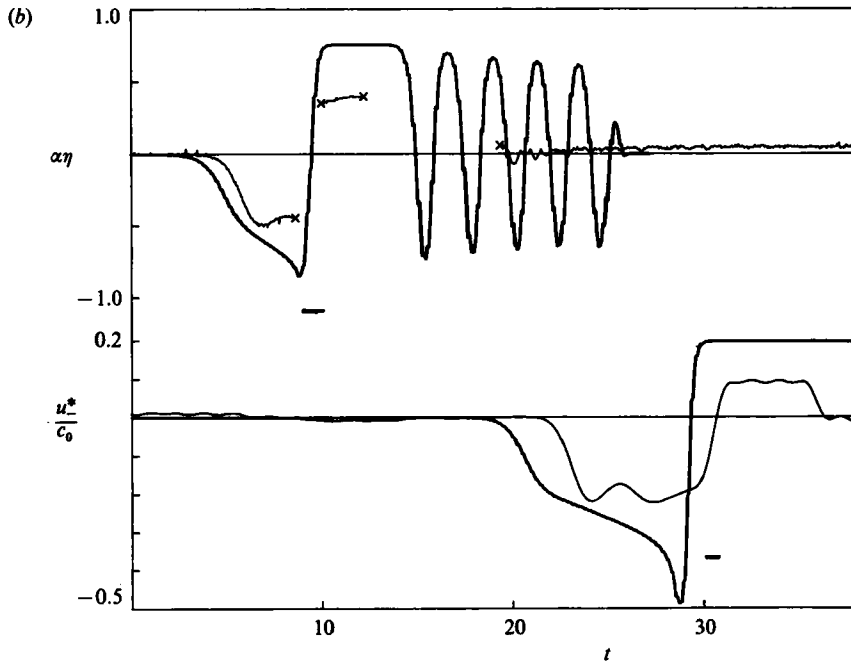
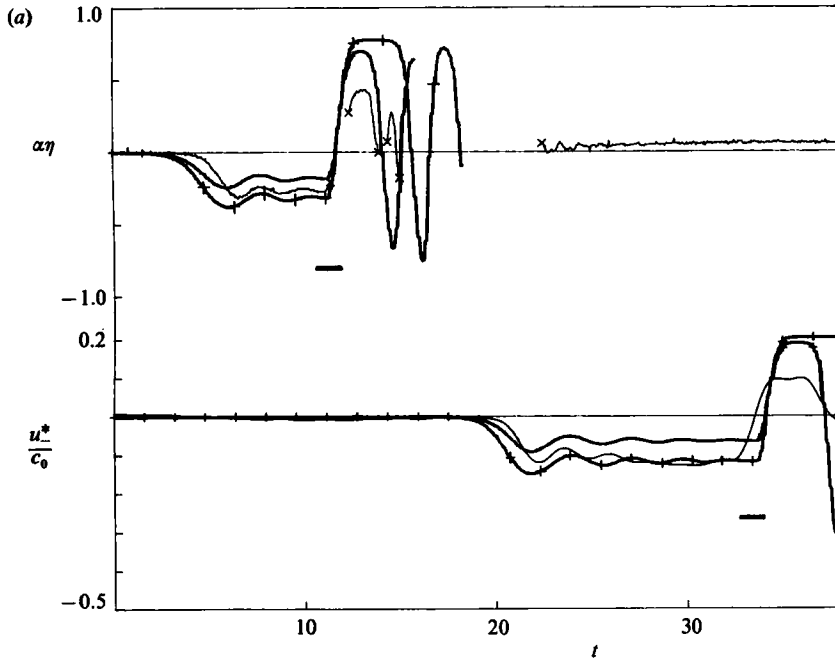


FIGURE 5(a, b). For caption see facing page.

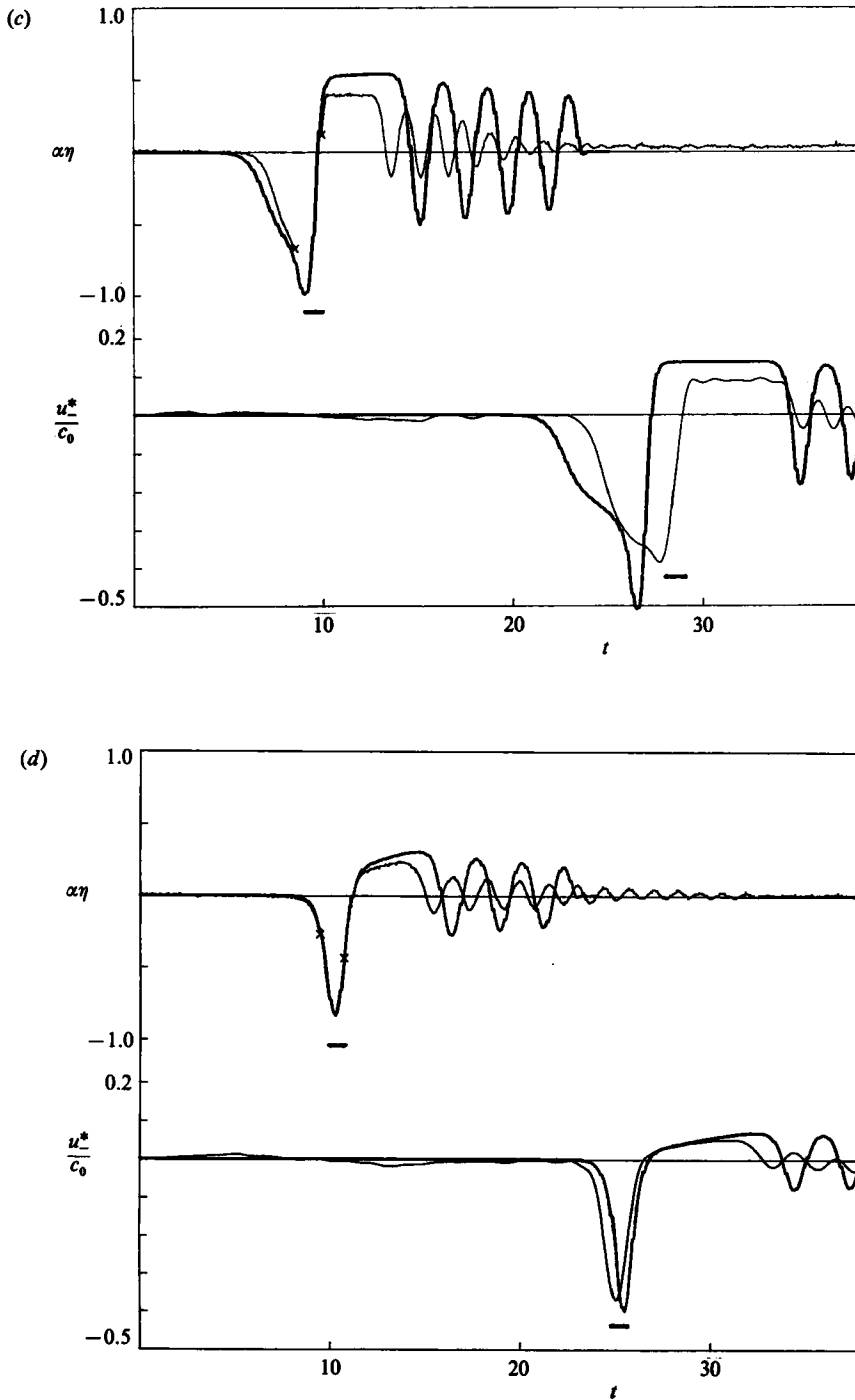


FIGURE 5. (a) Time series of interfacial displacement, $\alpha\eta$, and normalized velocity measured in the lower layer, u_1^*/c_0 , measured at 5 m and 9.25 m from the initial position of the carriage (light lines). Also shown are the corresponding numerical solutions to (2.12) with --- , $F = 0.73$; --- , 1.0, in the topographic forcing term (see text). $(F, R, \alpha, \beta, \gamma) = (0.73, 0.33, 0.51, 0.016, 0.3)$. (b) $F = 0.83$. (c) $F = 0.94$. (d) $F = 1.09$. The horizontal bars show the time of passage of the topography.

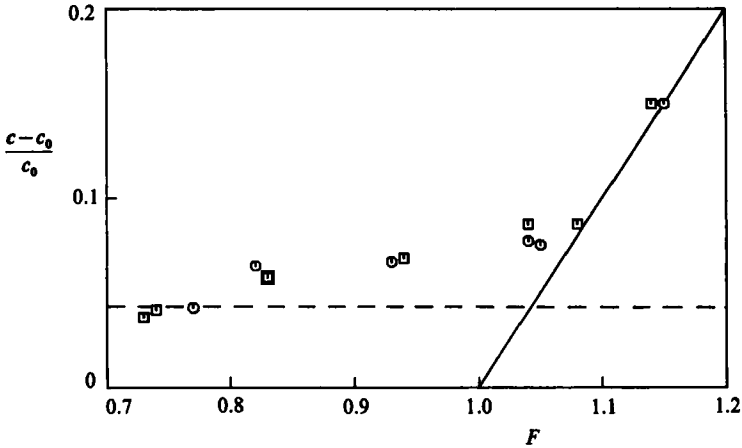


FIGURE 6. Measured nonlinear speed correction to upstream disturbances for $(R, \alpha, \beta) = (0.33, 0.51, 0.016)$, \square , $\gamma = 0.3$; \circ , $\gamma = 0.6$. Also shown is ----, $G(R)$ and —, $(F-1)$ (i.e. locally steady disturbance).

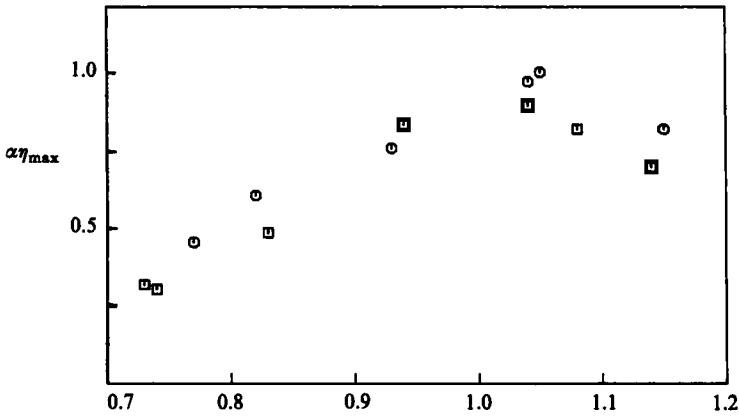


FIGURE 7. Measured maximum upstream disturbance amplitudes for $(R, \alpha, \beta) = (0.33, 0.51, 0.016)$, \square , $\gamma = 0.3$; \circ , $\gamma = 0.6$ (cf. figure 6).

4.4. Two-layer experimental and numerical results ($R = 0.2$)

Experiments were run with $R = 0.2$, $\gamma = 0.5$ and F in the range $[0.71, 1.31]$ and examples of the interfacial displacement and velocity in the lower layer are shown in figure 10 (cf. figure 5). Figure 10(a) ($F = 0.88$) shows the undular bore upstream with a trailing plateau and lee-wavetrain, in the interfacial displacement. The lee waves are not evident in the velocity signal further upstream. We believe that this is most likely due to the fact that these are short waves whose velocity eigenfunction has decayed significantly above the velocity measurement point. Figure 10(b) shows both experimental measurements and numerical solutions of the forced KdV equation for $F = 1.02$. Except for the prediction of an undular jump upstream and the length of the plateau following the topography, the agreement is poor. Figure 10(c) shows the experimental measurements at $F = 1.24$. The measurements, especially at the upstream station, appear to be approaching a steady supercritical state; however, as shown in figure 10(d) even at $F = 1.31$ the numerical solution is still

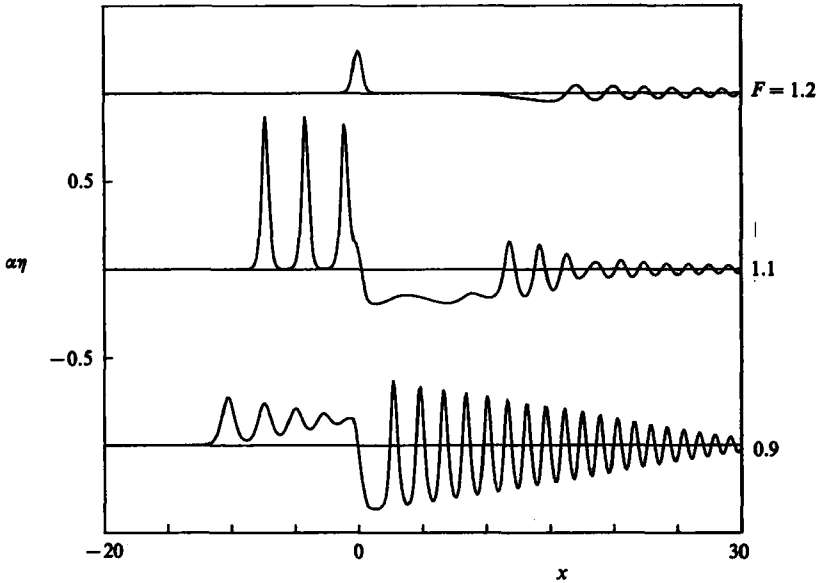


FIGURE 8. Examples of three classes of solutions to (2.12) neglecting the cubic term (inhomogeneous KdV equation) at $T = 0.5$: steady supercritical; sequence of solitary waves; undular upstream bore. $(R, \alpha, \beta, \gamma) = (0.2, 0.577, 0.0076, 0.0625)$.

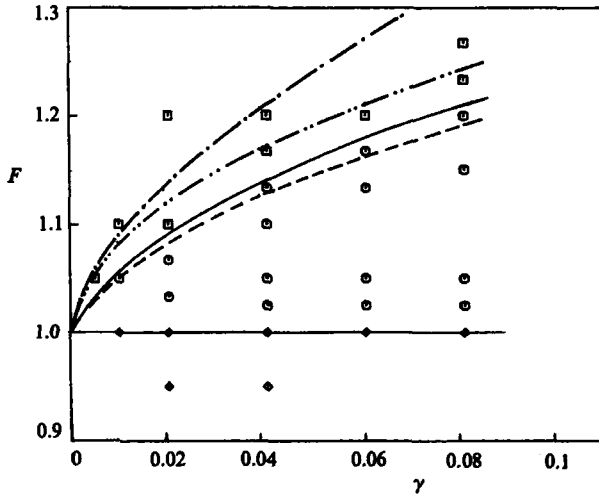


FIGURE 9. Regions in (F, γ) -plane occupied by solutions to inhomogeneous KdV equation: \square , locally steady supercritical solution; \circ , sequence of solitary waves upstream; \diamond , undular bore upstream. $(R, \alpha, \beta) = (0.2, 0.577, 0.0076)$. F_u (—) from Miles (1986) and equation (A 3); GS bounds: - - -, (5.3); - · - ·, (5.4).

unsteady relative to the topography showing a train of solitary waves evolving upstream while the measurements are essentially steady.

Figure 11 shows the measured non-dimensional excess speed and amplitude of the leading wave in the upstream disturbance. According to KdV theory with the scaling used, these points should be coincident. However, the measurements diverge significantly above $F = 0.9$ with the dimensionless leading wave amplitude $\alpha\eta_{\max}$ reaching a maximum of 1.6 at $F = 1.2$ before decreasing for larger F . The large

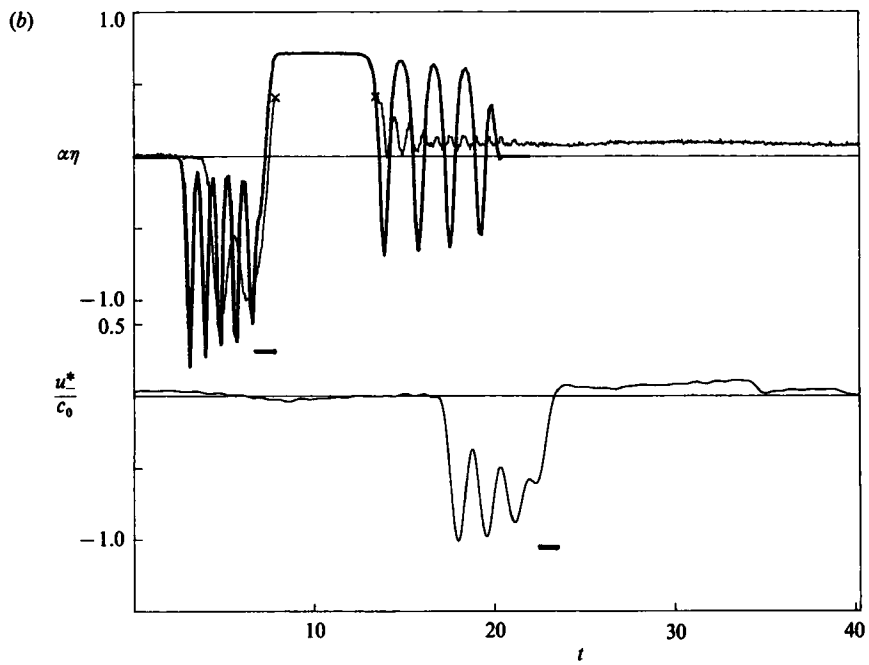
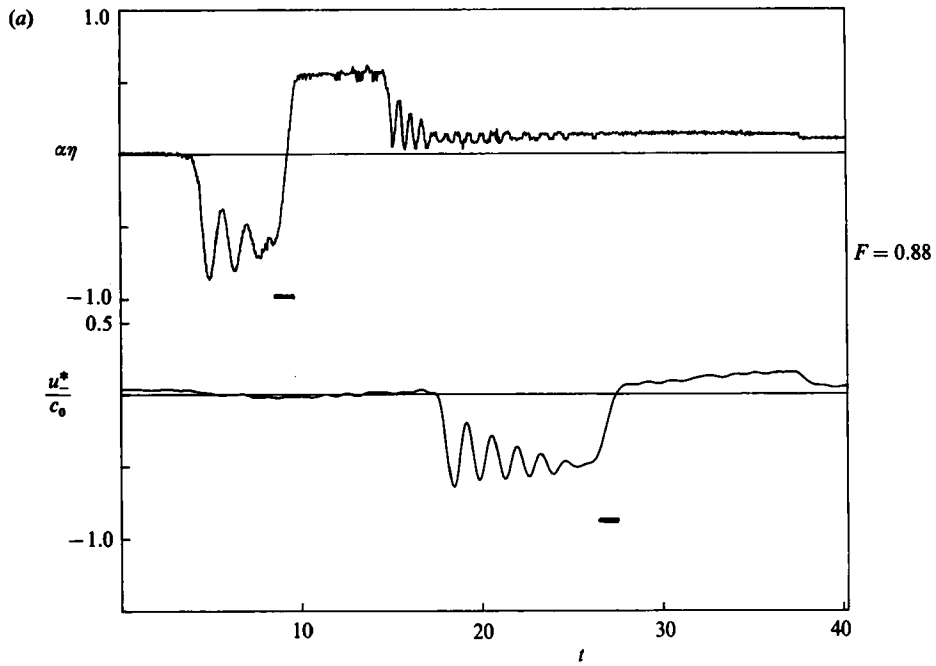


FIGURE 10 (a, b). For caption see facing page.

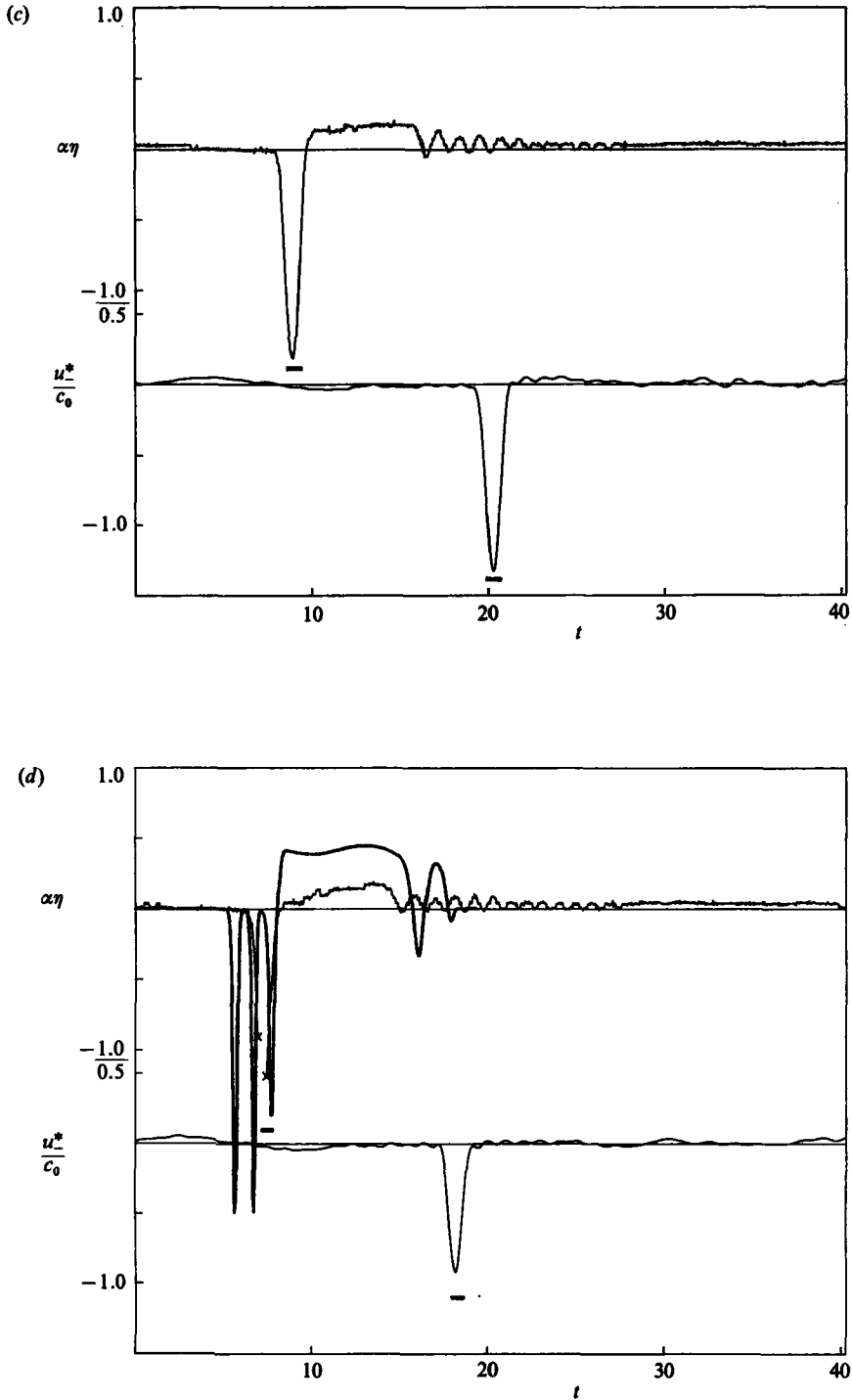


FIGURE 10. (a) Time series of interfacial displacement, $\alpha\eta$, and normalized velocity in the lower layer, u_*^*/c_0 , measured at 5 m and 9.25 m from the initial position of the carriage $(F, R, \alpha, \beta, \gamma) = (0.88, 0.2, 0.58, 0.007, 0.5)$. (b) As for (10a) except $F = 1.02$. Also shown is —, the numerical solution to the forced KdV equation. (c) As for (10a) except $F = 1.24$. (d) As for (10b) except $F = 1.31$. The horizontal bars show the time of passage of the topography.

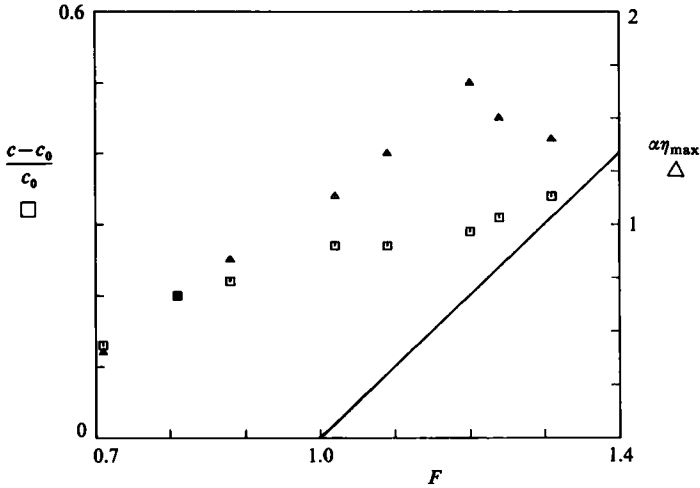


FIGURE 11. \square , measured nonlinear speed correction, and \triangle , amplitudes, of maximum in upstream disturbance for $(R, \alpha, \beta, \gamma) = (0.2, 0.58, 0.007, 0.5)$. Also shown is —, $(F-1)$; i.e. locally steady solution.

amplitudes here are clearly outside the range of weakly nonlinear theory and imply that higher order nonlinearities should be included.

It should also be noted that the apparently large values of the parameter α and the response of the interface ($\alpha\eta$) are due in part to the use of h_0 rather than $(d_+^* + d_-^*)$ for the vertical scale (cf. (2.20a)). Values of $\alpha\eta$ would be reduced by factors of 6.25 ($R = 0.2$) and 4.5 ($R = 0.33$) if the total depth were used as the vertical scale. Improved comparisons between the predictions and the experimental measurements may also be realized by relaxing the Boussinesq approximation; however, these should only be small since the errors are only of $O(1 + \Delta\rho/\rho)$ in the highest-order terms.

5. Discussion

The primary aim of this paper has been to consider the use of inhomogeneous KdV and EKdV equations as models of transcritical two-layer flow over topography. Comparison of the two model equations over the range of parameters considered shows that they both display qualitatively similar supercritical locally-steady solutions, and subcritical solutions with undular bores propagating upstream. However, their behaviour in the transcritical regime is markedly different for the parameter ranges considered. While the homogeneous EKdV equation has two classes of solitary wave solutions only the monotonic solution appears upstream of the topography in the transcritical regime. This contrasts with the inhomogeneous KdV equation which displays a sequence of Boussinesq solitary waves upstream in some neighbourhood of critical flow.

The predictions of the inhomogeneous EKdV equation appears to be confirmed, at least for a limited range of experimental conditions with $R = 0.33$. Due to the thinner upper layer it was not possible to completely satisfy the theoretical assumption of weak forcing for cases in which the inhomogeneous KdV equation was expected to apply ($R = 0.2$). However, it is possible to compare our results with the recent analytical and numerical work of Grimshaw & Smyth (1986; hereinafter referred to as GS) and Smyth (1987; hereinafter referred to as S). GS considered the

more general case of continuously stratified fluid and derived an equation (GS (4.2a)) equivalent to (2.12) without the cubic term. For positive forcing (the case considered here), GS postulated the existence of four regimes, based on the value of a detuning parameter Δ , which in our notation is given by

$$\Delta = (F-1) \left[\frac{8d_- - 1}{d_- \gamma} \right]^{\frac{1}{2}}. \quad (5.1)$$

In table 1 we have listed the GS regimes for the inhomogeneous KdV equation along with their characterization of the upstream solution, and the regime boundaries for our numerical solutions in figures 3 and 8. (In figure 3 we are comparing their classification with the solutions to the inhomogeneous EKdV equation.) From table 2, we see that their classification for broad obstacles appears to show reasonable agreement with our results in figure 8; perhaps with the exception of the solution at $F = 1.2$, which appears to be supercritical but falls into the GS resonant regime. In contrast GS would characterize all of figure 3 as resonant. Further, their resonant regime requires a train of identical (Boussinesq) solitary waves upstream.

We can also compare the GS regimes with our extension of Miles' (1986) prediction of the transcritical regime in which the hypothesis of steady flow fails. In the terminology of GS, this transcritical regime is defined by $\Delta_{-}^{(1)} < \Delta < \Delta_{+}^{(2)}$, and is in agreement with (A 3), and in figure 9 corresponds to

$$-1.76\gamma^{\frac{1}{2}} < (F-1) < 1.11\gamma^{\frac{1}{2}}. \quad (5.2)$$

In contrast, the GS bounds Δ_{+} and Δ_{-} are given by

$$-0.88\gamma^{\frac{1}{2}} < (F-1) < 1.76\gamma^{\frac{1}{2}}, \quad (5.3)$$

for narrow obstacles, and

$$-0.42\gamma^{\frac{1}{2}} < (F-1) < 0.84\gamma^{\frac{1}{2}}, \quad (5.4)$$

for broad obstacles. We have plotted the upper bounds of (5.3) and (5.4) in figure 9. The latter shows moderate to good agreement with our numerical results.

The approximate analytical results of GS were corrected by S, who showed that the upstream solution in the resonant regime was not a train of identical solitary waves, but rather a train of modulated cnoidal waves with the wave at the leading edge of the upstream disturbance having a modulus 1 and hence corresponding to a solitary wave. In figure 12 we show a comparison of the amplitude of the leading wave in our upstream disturbance (see figures 7, 10 and 11) plotted against the results of GS (figure 6a) and S (figure 1). Also shown are our corresponding numerical results for figure 10(a, b, d). The agreement between the numerical results and experimental measurements for $R = 0.2$ is poor for smaller Δ , improves as Δ approaches unity and then deteriorates again as Δ increases further. For larger Δ the experiments appear to show a more rapid approach to a steady supercritical solution, while the numerical solutions still show solitary waves propagating upstream. There is no agreement between the GS numerical results and our measurements for $R = 0.33$. This contrasts with the relatively good agreement between the numerical and experimental results of figure 5. Notwithstanding the relatively good agreement between the leading wave amplitude and the numerical solutions for $0 < \Delta < 1$, $R = 0.2$, figure 10 reveals significant quantitative differences in the upstream disturbance. Unfortunately, Smyth restricted the comparison of his analytical solution with the numerical solutions of GS to the leading-wave amplitude.

Where direct comparisons are possible, our experimental results appear to agree with those of Baines (1984). In figure 13 we compare our measurements of upstream

Regime	Upstream solution	Narrow obstacle			
		Δ	Broad obstacle	Figure 3	Figure 8
I. Subcritical	'Finite number of upstream solitary waves'	$\Delta < \Delta_-$	$\Delta < -3.46$	-3.37	-4.53
II. Transition to resonant	'Modulated cnoidal wavetrain'	$\Delta_- < \Delta < \Delta_+$	$-3.46 < \Delta < -1.73$	$(-3.37, -1.69)$	$(-4.53, -2.26)$
III. Resonant	'Train of solitary waves of uniform amplitude'	$\Delta_- < \Delta < \Delta_+$	$-1.73 < \Delta < 3.46$	$(-1.69, 3.37)$	$(-2.26, 4.53)$
IV. Supercritical	No influence	$\Delta > \Delta_+$	$\Delta > 3.46$	3.37	4.53

TABLE 1. Flow regimes due to Grimshaw & Smyth (1986) and predicted regime boundaries in figures 3 and 8

Figure 3		Figure 8	
F	Δ	F	Δ
0.95	-1.37 (III)	0.9	-1.72 (II-III)
1	0 (III)	1.1	1.56 (III)
1.1	2.73 (III)	1.2	2.98 (III)

TABLE 2. Grimshaw & Smyth's detuning parameter, Δ , and flow regime (according to table 1) for figures 3 and 8

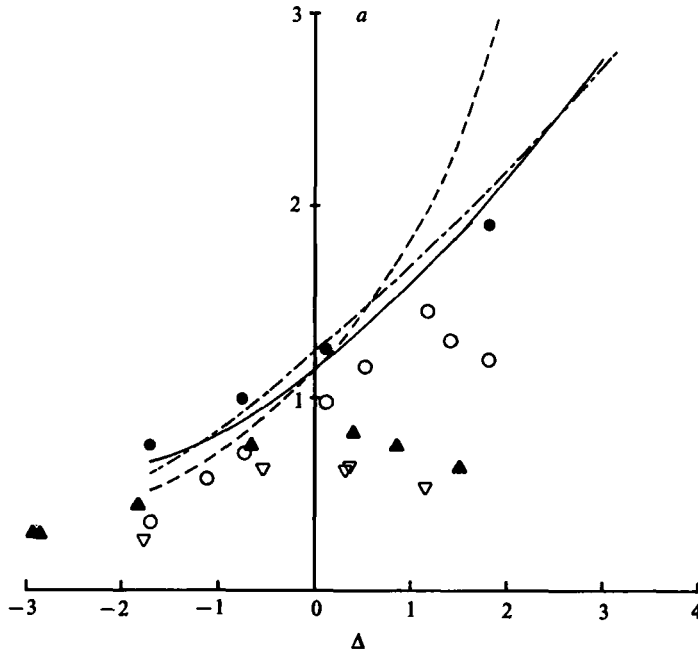


FIGURE 12. Dependence of the leading upstream wave amplitude, a , on Δ , the GS detuning parameter (S, figure 1). \circ , experimental measurements, and \bullet , numerical predictions, for $R = 0.2$ (cf. figures 10, 11). Experimental measurements for $R = 0.33$, with \blacktriangle , $\gamma = 0.3$, and ∇ , $\gamma = 0.6$. —, GS numerical solution, and - - -, hydraulic approximation (cf. GS, figure 6a). — · —, Smyth's (1987) modulation theory (cf. S, figure 1).

bore amplitude versus speed for $R = 0.2, 0.35$ (0.33)† and jump height versus Froude number for $R = 0.2$. In figure 13(a) it is evident that our measurements are within the scatter of Baines'. Our measurements of the bore amplitude versus Froude number for $R = 0.2$ fall a little below Baines' and are for a slightly larger relative topographic height. Nevertheless, for experiments of this kind the agreement should be considered good. Unfortunately, Baines did not show comparable data for $R = 0.35$.

Given this agreement with Baines (1984), and the agreement between the inhomogeneous EKdV model and our experiments for $R = 0.33$, it appears that Baines' observation of dissipationless bores and rarefactions are consistent with our observations and the predictions of the EKdV model. Baines' conjecture regarding the impossibility of inviscid bores in two-layer systems is not supported by these results.

The existence of a globally unsteady transcritical regime for these inhomogeneous equations points to the need for caution in attempting to use steady hydraulic models in related flows. Even the solutions which attain a locally steady form in the neighbourhood of the topography do so only after a long time. In particular, for all the flows considered here, locally steady solutions are only attained after a time $T = O(1)$. In the context of coastal oceanography in which d_+^* , d_-^* may be $O(10^2 \text{ m})$, $l \approx O(10^3 \text{ m})$ and $c_0 \approx O(1 \text{ ms}^{-1})$, this can lead to times of about 1–10 days for locally steady flows to be established.

The solutions to the inhomogeneous EKdV equation would appear to present a

† The differences between our measurements for $R = 0.33$ and Baines' for $R = 0.35$ should be small.

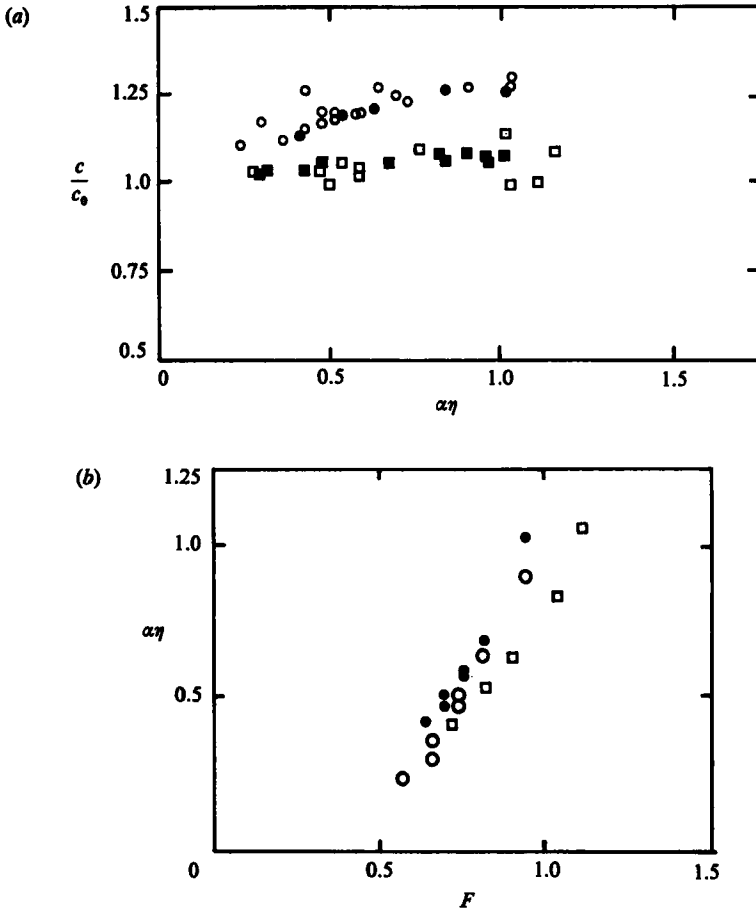


FIGURE 13. (a) Plot of measured upstream bore speed versus amplitude for \bullet , $R = 0.2$, and \blacksquare , $R = 0.33$. Open symbols are corresponding data from Baines (1984, figure 12) for \circ , $R = 0.2$ and \square , 0.35 respectively. (b) Measured upstream bore amplitude versus Froude number for \square , $R = 0.2$, $\gamma = 0.5$ compared with corresponding measurements of Baines (1984, figure 20c) for \circ , $\gamma = 0.32$; \bullet , 0.4 .

novel mechanism for frontogenesis, with the monotonic dissipationless bores providing a frontal transition. While these are propagating-wave solutions, their speed relative to the topography in the transcritical regime is small (cf. figure 1) and in nature they may appear as quasi-steady features. This model may also have some application in meteorology with regard to orographic fronts.

Finally, the symmetry properties of the homogeneous form of equation (2.15) afford a novel form of solitary wave. Miles (1981) showed that the homogeneous form of (2.15) is invariant under the transformation

$$\eta_* = 1 - \eta.$$

Thus if η is a forward-facing bore of amplitude unity (2.18a),

$$\eta_* = \frac{1}{2}(1 - \tanh \theta),$$

and corresponds to a rearward-facing bore. We anticipated that in that parametric regime in which the forward-facing bore was realized upstream of the topography,

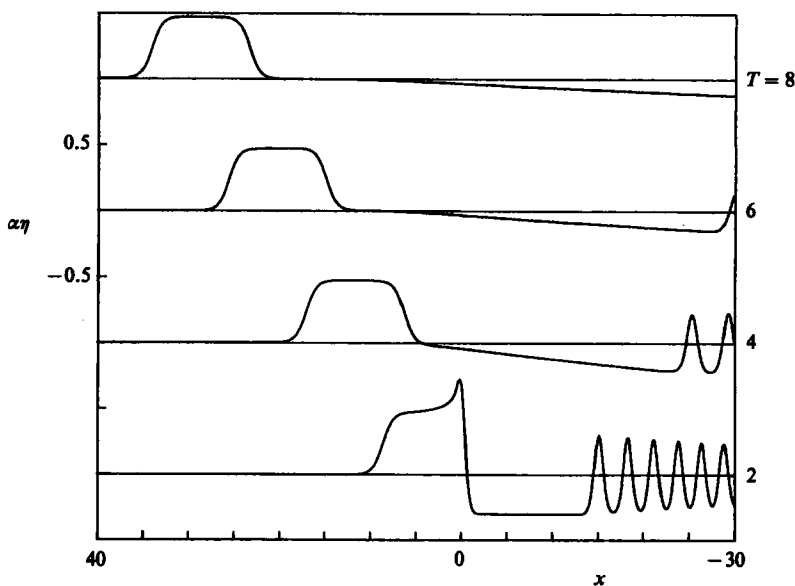


FIGURE 14. Solutions to (2.12) with topography given by $H = H(x) \mathcal{H}(0) \mathcal{H}(2-T)$ where \mathcal{H} is the Heaviside unit step function. Note that a solitary wave bound by forward- and rearward-facing monotonic bore solutions is generated upstream $(F, R, \alpha, \beta, \gamma) = (0.988, 0.35, 0.472, 0.0154, 0.092)$.

cessation of the topographic forcing may lead to the complementary bore at the rear of the upstream disturbance. An example of such a numerical experiment is shown in figure 14. Here the forcing was initiated at time $T = 0$ and terminated at $T = 2$. A plateau of permanent form evolves upstream with the bore solutions at the front and rear. Since the time of cessation of the forcing is arbitrary the length of the solitary wave so formed is also arbitrary. Thus it is possible to generate solitary waves of arbitrary length in contrast to the Boussinesq solitary wave, for which there is a relationship between the wave amplitude and length.

We thank Elizabeth Macomb for assistance with the experiments. This research was supported by the Office of Naval Research (Coastal Studies).

Appendix. Unsteady transcritical flow

Miles (1986) has recently shown that with scaling assumptions for nonlinearity, dispersion and transcritical forcing consistent with those made in §2 and (2.7), the hypothesis of steady flow past an obstacle fails for the single-layer flow in a shallow canal of upstream depth D if $F \equiv U/(gD)^{1/2}$ is in the transcritical regime

$$1 - \left(\frac{9A}{2D^2}\right)^{1/2} < F^2 < 1 + \left(\frac{9A}{4D^2}\right)^{1/2}, \quad (\text{A } 1)$$

where A is the cross-sectional area of the transverse obstacle. The corresponding evolution equation for the dimensionless surface elevation is

$$\eta_t + (F-1)\eta_x - \frac{3}{2}\alpha\eta\eta_x - \frac{1}{6}\beta\eta_{xxx} = \frac{1}{2}\beta BFH_x \quad (\text{A } 2)$$

where the normalization corresponds to (2.6) with $h_0 = \sigma = 1$.

Now (2.12) without the cubic term, may be renormalized to match (A 2). Therefore,

any conclusion based on (A 2) will also apply to the two-layer case under renormalization.

It is a simple matter to show that if (A 1) holds true for the two-layer KdV case, the hypothesis of steady transcritical flow fails in the transcritical regime

$$F_1^2 \equiv 1 + \left(\frac{9\mathcal{A}}{2h_0^2} \right)^{\frac{2}{3}} < F^2 < 1 + \left(\frac{9\mathcal{A}}{4h_0^2} \right)^{\frac{2}{3}} \equiv F_u^2, \quad (\text{A } 3)$$

where

$$\mathcal{A} = \left(\frac{d_{-2}}{d_{-1}d_1^{\frac{1}{2}}} \right) A. \quad (\text{A } 4)$$

Thus the effect of the stratification is to change the effective area of the topography.

REFERENCES

- AKYLAS, T. R. 1984 On the excitation of long nonlinear water waves by a moving pressure distribution. *J. Fluid Mech.* **141**, 455–466.
- BAINES, P. G. 1984 A unified description of two-layer flow over topography. *J. Fluid Mech.* **140**, 127–167.
- BENJAMIN, T. B. 1966 Internal waves of finite amplitude and permanent form. *J. Fluid Mech.* **25**, 241–270.
- COLE, S. L. 1985 Transient waves produced by flow past a bump. *Wave Motion* **7**, 579–587.
- GRIMSHAW, R. H. J. & SMYTH, N. 1986 Resonant flow of a stratified fluid over topography. *J. Fluid Mech.* **169**, 429–464.
- HELFRICH, K. R., MELVILLE, W. K. & MILES, J. W. 1984 On interfacial solitary waves over slowly varying topography. *J. Fluid Mech.* **149**, 305–317.
- KAKUTANI, T. & YAMASAKI, N. 1978 Solitary waves on a two-layer fluid. *J. Phys. Soc. Japan* **45**, 674–679.
- LEE, C. Y. & BEARDSLEY, R. C. 1974 The generation of long nonlinear internal waves in a weakly stratified shear flow. *J. Geophys. Res.* **7**, 338–346.
- LONG, R. R. 1954 Some aspects of the flow of stratified fluids. Part 2. *Tellus* **6**, 97–115.
- MAXWORTHY, T. 1979 A note on the internal solitary waves produced by tidal flow over a three-dimensional ridge. *J. Geophys. Res.* **84**, 338–346.
- MEI, C. C. 1986 Radiation of solitons by slender bodies advancing in a shallow channel. *J. Fluid Mech.* **162**, 53–67.
- MILES, J. W. 1979 On internal solitary waves. *Tellus* **31**, 456–462.
- MILES, J. W. 1981 On internal solitary waves. II. *Tellus* **33**, 397–401.
- MILES, J. W. 1986 Stationary, transcritical channel flow. *J. Fluid Mech.* **162**, 489–499.
- SMYTH, N. F. 1987 Modulation theory solution for resonant flow over topography. *Proc. R. Soc. Lond. A* **409**, 79–97.
- VLEIGHNART, A. C. 1971 On finite difference methods for the Korteweg de Vries equation. *J. Engng Maths.* **5**, 137–155.
- WHITHAM, F. B. 1974 *Linear and Nonlinear Waves*. Academic.
- WU, D. M. & WU, T. Y. 1982 Three-dimensional nonlinear long waves due to moving surface pressure. *Proc. 14th Symp. Naval Hydrodyn.* pp. 103–129.